ARTICLE

Check for updates

Simulating graphene dynamics in synthetic space with photonic rings

Danying Yu[1,8], Guangzhen Li [1,8], Meng Xiao [2], Da-Wei Wang [3], Yong Wan[4], Luqi Yuan [1✉] & Xianfeng Chen[1,5,6,7]

Photonic honeycomb lattices have attracted broad interests for their fruitful ways in manipulating light, which yet hold difficulties in achieving arbitrary reconfigurability and hence flexible functionality due to fixed geometry configurations. Here we theoretically propose to construct the honeycomb lattice in a one-dimensional ring array under dynamic modulations, with an additional synthetic dimension created by connecting the frequency degree of freedom of light. Such a system is highly re-configurable with parameters flexibly controlled by external modulations. Therefore, various physical phenomena associated with graphene including Klein tunneling, valley-dependent edge states, effective magnetic field, as well as valley-dependent Lorentz force can be simulated in this lattice, which exhibits important potentials for manipulating photons in different ways. Our work unveils an alternative platform for constructing the honeycomb lattice in a synthetic space, which holds complex functionalities and could be important for optical signal processing as well as quantum simulation.

[1] State Key Laboratory of Advanced Optical Communication Systems and Networks, School of Physics and Astronomy, Shanghai Jiao Tong University, 200240 Shanghai, China. [2] Key Laboratory of Artificial Micro- and Nano-Structures of Ministry of Education and School of Physics and Technology, Wuhan University, 430072 Wuhan, China. [3] Interdisciplinary Center for Quantum Information and Zhejiang Province Key Laboratory of Quantum Technology and Device, Department of Physics, Zhejiang University, 310027 Hangzhou, China. [4] National Institute of Metrology, 102200 Beijing, China. [5] Shanghai Research Center for Quantum Sciences, 201315 Shanghai, China. [6] Jinan Institute of Quantum Technology, 250101 Jinan, China. [7] Collaborative Innovation Center of Light Manipulations and Applications, Shandong Normal University, 250358 Jinan, China. [8] These authors contributed equally: Danying Yu, Guangzhen Li. ✉email: yuanluqi@sjtu.edu.cn

Honeycomb lattices, possessing the same geometry as graphene[1,2], have attracted great interest in condensed matter physics[3,4] and photonics[5,6]. Rich physical phenomena have been reported in photonic honeycomb lattices, taking advantage of properties of Dirac points and the valley degree of freedom[6–15] and showing an excellent platform for studying topological photonics[16], which also have potential applications in the interface of nonlinear optics[17] and quantum optics[18], pointing towards topological fiber[19], topological laser[20], as well as edge and gap solitons[21]. Different platforms have been achieved to construct photonic honeycomb lattices, such as waveguide arrays[22], on-chip silicon photonics[23], semi-conductor microcavities[24], and metamaterials[25]. However, one notes that the reconfigurability and flexible experimental feasibility of a system are attractive for satisfying various experimental requirements and different applications, as well as relaxing the fabrication constrains, which are naturally limited in the current honeycomb systems due to their fixed configurations or structures after fabrication[22–25]. Therefore, it is of significant importance to find an alternative platform, which is experimentally feasible and holds reconfigurability.

Recently, synthetic dimensions have experienced extensive explorations in many areas of photonics, for providing exotic connectivities and exploring physics beyond real dimensions, in which a photonic synthetic dimension can be formed by coupling suitable degrees of freedom of light, such as frequency modes, orbital angular momenta, modal dimensions, and others[26–28]. Among the various platforms to construct synthetic dimensions, a ring resonator under dynamic modulation has been found to be capable of creating a synthetic dimension along the frequency axis of light[29], which together with spatial dimensions, a variety of physical implementations have been suggested with two or more dimensions[30–39].

Here, we theoretically propose the construction of a highly reconfigurable honeycomb lattice in a synthetic space in a modulated ring resonator system. We show that a one-dimensional ring resonator array composed by two types of resonators under appropriate dynamic modulation supports a two-dimensional honeycomb lattice in a synthetic space including both spatial and frequency dimensions. Different physics associated with the photonic graphene can be simulated in this unique platform, such as Klein tunneling[14], valley-dependent edge states[13], topological edge states with the effective magnetic field[40], and valley-dependent Lorentz force[8]. The modulated ring systems can be realized in either fiber-based system[41–44] or on-chip lithium niobate resonator[45], which brings our proposal to a flexible experimental setup with state-of-art technologies in bulk optics or integrated photonics. Our work not only broadens the current research on synthetic dimensions in photonics[26,27], but also enriches quantum simulations with topological photonics[46,47], which shows potential applications in optical signal processing[48,49] and quantum computations[50,51].

Results

Model. We begin with considering a pair of ring resonators (labeled as A and B) with the same circumference L undergoing dynamic modulation [Fig. 1a]. The central resonant frequencies of ring A and ring B are set at ω_0 and $\omega_0 - \Omega/2$, respectively. In the absence of group velocity dispersion (GVD) in waveguides that compose rings, the frequency of the mth resonant mode in ring A (ring B) is $\omega_{m,A} = \omega_0 + m\Omega$ ($\omega_{m,B} = \omega_0 - \Omega/2 + m\Omega$), where $\Omega = 2\pi v_g/L$ is the free spectral ranges (FSR) with v_g being the group velocity inside both rings. The approximation that GVD of waveguides is zero makes the synthetic frequency dimension being uniform, which is valid for considering finite

resonant modes near the zero GVD point and is confirmed by previous experiments[41–44]. We place electro-optic modulators (EOM) inside two rings, with modulation frequency $\Omega/2$ and modulation phase ϕ. A synthetic frequency dimension with the effective hopping amplitude g can be constructed with spaced frequency $\Omega/2$ in the frequency axis of light, where modes supported by rings A and B are labeled by a and b, respectively. With the building block for constructing the one-dimensional synthetic frequency dimension in a pair of rings, we can then use it to construct a synthetic honeycomb lattice in a one-dimensional array of pairs of rings shown in Fig. 1b [see "Methods" section]. The ring array consists groups of rings ($n = 1, 2, \ldots, N$), each of which contains two pairs of rings with different combinations, i.e., AB (labeled as $\alpha = 1$) and BA (labeled as $\alpha = 2$), respectively. We write the Hamiltonian of the system under the first-order approximation:

$$
\begin{aligned}
H_r = \sum_{m,n} \Big[& \kappa(a^\dagger_{n,m,1} a_{n-1,m,2} + b^\dagger_{n,m,2} b_{n,m,1}) \\
& + g_{2n-1}(a^\dagger_{n,m,1} b_{n,m,1} e^{i\phi_{2n-1}} + a^\dagger_{n,m,1} b_{n,m+1,1} e^{-i\phi_{2n-1}}) \\
& + g_{2n}(b^\dagger_{n,m,2} a_{n,m-1,2} e^{i\phi_{2n}} + b^\dagger_{n,m,2} a_{n,m,2} e^{-i\phi_{2n}}) \Big] + h.c.,
\end{aligned}
\tag{1}
$$

where $a^\dagger_{n,m,\alpha}$ ($a_{n,m,\alpha}$) and $b^\dagger_{n,m,\alpha}$ ($b_{n,m,\alpha}$) are corresponding creation (annihilation) operators, and κ is the evanescent-wave coupling strength between two rings at the same type. The Hamiltonian in Eq. (1) therefore supports a two-dimensional synthetic honeycomb lattice [Fig. 1c].

The honeycomb lattice is constructed in a synthetic space including the spatial (x) and frequency (f) dimensions. Different from conventional photonic honeycomb lattice in real space[13,14] that depends greatly on apparent geometry, the synthetic honeycomb lattice in Eq. (1) is dependent on both couplings between rings (κ) and modulations (g_i). Therefore, without loss of generality, we label the horizontal distance in the synthetic lattice between two sites with the same types as d and the horizontal distance between two sites with different types as $d/2$ along the x axis in the later plots of field patterns. The flexible choice of hopping amplitude g_i and phase ϕ_i provides powerful reconfigurability toward different physical phenomena in simulating graphene dynamics. We first consider $\kappa = g_i = g$ and $\phi_i = 0$, and the synthetic lattice holds the unit cell with the translation symmetry including two frequency modes a and b in two rings. The band structure of this honeycomb lattice in the first Brillouin zone can be plotted in the k_x–k_f space, where k_x and k_f are wave vectors reciprocal to the spatial (x) and frequency (f) axes, respectively. Dirac point K and K' at $(k_x, k_f) = (0, \pm 4\pi/3\Omega)$ can be seen in the band structure in Fig. 1d, where the zoomed-in Dirac cone shows linear dispersion near K' point [Fig. 1e]. In the following, we will show the capability for achieving different phenomena associated with the honeycomb lattice with the current platform.

Klein tunneling. Klein tunneling, as an intriguing phenomenon in physics exploring a particle passing through a barrier higher than its energy, has experienced great interest in different platforms including graphene and photonic/phononic crystals[7,14,52,53]. To demonstrate such physics in the synthetic honeycomb lattice in Fig. 1c, we couple the first (A_1) and the last (A_{2N}) rings with an external waveguide such that a periodic condition along the x axis can be naturally created. Such a design forms a carbon-nanotube-like shape [Fig. 2a]. In simulation, we consider $N = 12$, which corresponds to 48 rings ranging inside $x \in [0, 35d]$, and modes in the region $f \in [-8\Omega, 47.5\Omega]$. Here we refer $f = 0$ to $\omega_{0,B}$ and denote the first (A_1) ring as $x = 0$ for the simplicity. We first excite the honeycomb lattice by injecting an input plane wave with
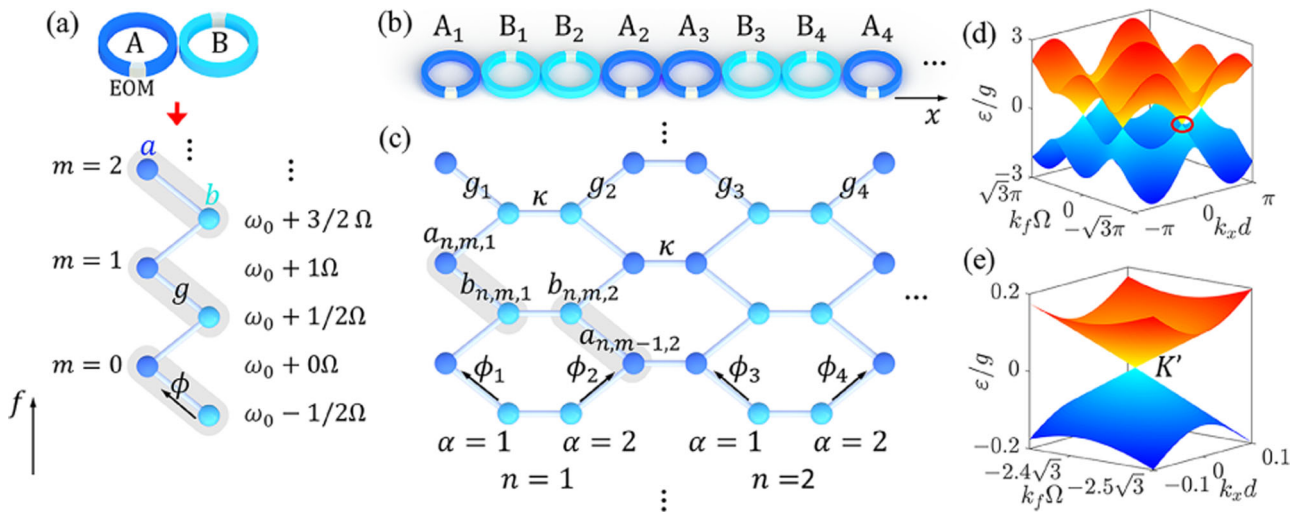
Fig. 1 Construction of synthetic honeycomb lattice. a Rings A and B support a set of resonant modes a (blue circle) and b (cyan circle) separated by the free spectral range Ω in the frequency dimension (f). Both rings are modulated by electro-optic modulator (EOM) with modulation phase ϕ, modulation frequency $\Omega/2$, and effective hopping amplitude g. ω_0 and $\omega_0 - \Omega/2$ are central resonant frequencies of ring A and ring B. m denotes the index of the mth resonant mode. **b** A one-dimensional array of ring resonators is composed of groups of pairs of rings in **a** along the spatial dimension x. A_i (B_i) represents the ith ring A (ring B), where i is a positive integer. **c** The system in **b** can be mapped into a honeycomb lattice in a synthetic space including one spatial dimension (x) and one frequency dimension (f). $a_{n,m,\alpha}$ and $b_{n,m,\alpha}$ represent the operator for the field at the mth mode in ring A and ring B, which are labeled by integers n and α as indicated in the figure. g_i and ϕ_i are the corresponding effective hopping amplitude and modulation phase, while κ is the coupling strength. **d** The band structure of the honeycomb lattice in the reciprocal space (k_x, k_f), where k_x and k_f are wave vectors reciprocal to spatial and frequency axes, ε is the eigenvalue (frequency shift of the field), and d denotes the horizontal distance between two sites with same types in the synthetic lattice. **e** The zoomed-in Dirac cone at K' point in **d**.

distribution of $s_1 = e^{-(f-f_0)^2/\Delta^2} e^{ik_x(x-x_0)+ik_f(f-f_0)}$ to excite the initial wave packet of the field shown in Fig. 2b, where $f_0 = 39\Omega$, $x_0 = 17.5d$, and $\Delta = 8.95\Omega$, and collect signals through external waveguides to readout the evolution of the field in the synthetic honeycomb lattice [see "Methods" section]. We set the k-vector in s_1 in the vicinity of the Dirac point K by using $(k_x, k_f) = (0, 4.04\pi/3\Omega)$. The corresponding frequency detuning of the source is $\varepsilon = 0.036g$, which falls in the linear dispersion region in the Dirac cone as indicated in Fig. 1d and gives the initial velocity of the wave packet along the negative k_f direction. The simulation verifies this feature, that the field propagates to the bottom of the synthetic honeycomb lattice at $t = 42g^{-1}$ as shown in Fig. 2c without distortion in shape, since there is no barrier in this case.

Based on the calculation in Fig. 2c, we set an artificial square-shape barrier in the middle range of the frequency dimension in the synthetic honeycomb lattice as shown in Fig. 2d, which in principle can be achieved by adding on-site potential terms $Va_{n,m,\alpha}^\dagger a_{n,m,\alpha}$ and $Vb_{n,m,\alpha}^\dagger b_{n,m,\alpha}$ in the range $f \in [12, 35.5]\Omega$. We first consider the case with $V = 0.05g$ which gives $\varepsilon < V$. The field experiences an effective lift in its energy in the barrier region, but still sticks to the linear region of the Dirac cone, so the initial negative group velocity does not change during this process [Fig. 2d]. This is indeed verified in the simulation in Fig. 2e, which shows that the field propagates to the bottom of the synthetic honeycomb at $t = 42g^{-1}$ without significant change in the field distribution. As a comparison, we take a larger potential $V = 1.5g$, outside of the linear region of the Dirac cone, where the field propagation is distorted as shown in Fig. 2f.

The artificial square-shape barrier along the frequency axis of light is not easy to be constructed in the frequency dimension. In the waveguide that composes the ring, there exists the group velocity dispersion that can introduce on-site potentials at modes with different resonant frequencies[34,54]. We now take the dispersion back into the consideration only in this part, with the zero dispersion point at $f_1 = 23.75\Omega$. The modulation

frequency is chosen to be resonant with the frequency spacing between modes near $f = 8.5\Omega$ (and 39Ω), which results in an effective parabola-shape potential barrier $V(f) = 0.05g + 2D(f/\Omega - f_1/\Omega)^2$ with $D = -1.075 \times 10^{-4}g$ [Fig. 2g]. Such the group velocity dispersion can be designed by the waveguide-structure engineering[55]. Note here the maximum value of the barrier (V_{max}) is $0.05g > \varepsilon$. Different from the previous case in Fig. 2d that the field experiences a sudden change in the synthetic k-space, when the wave packet of the field propagates toward the bottom of the synthetic lattice, it experiences a gradual change inside the Dirac cone. Yet, the distribution of the wave packet still remains largely unchanged at $t = 42g^{-1}$, as one sees in Fig. 2h. The propagation of the field is distorted if one uses a larger barrier, i.e., beyond the limit of the Dirac cone as shown in Fig. 2i, where the simulation is performed with $V_{max} = 1.5g$. Therefore, as long as the potential change is limited inside the linear region near the Dirac point, the constructed synthetic honeycomb lattice supports the Klein tunneling along the frequency axis of light.

Valley-dependent edge state. Valley-dependent photonic phenomena recently attract a broad interest in photonics for providing valley degree of freedom, which offers a new possibility to manipulate light and finds important applications in optical encoding and enlarging the optical information capacity[13]. Here we show the existence of valley-dependent edge states in the synthetic space. Lengths of rings are carefully adjusted to introduce the required effective on-site potential in each ring, which breaks the inversion symmetry of the synthetic lattice and lifts the degeneracy at Dirac points K and K'.

We consider 12 pairs of rings (24 rings), each of which has a different circumference L' close to the reference length L. The offset in length leads to slightly shifted resonant frequencies in each ring, which leads to the effective on-site potential on each column site in the synthetic lattice as shown in Fig. 3a [see "Methods" section]. As one can see, we consider that there are
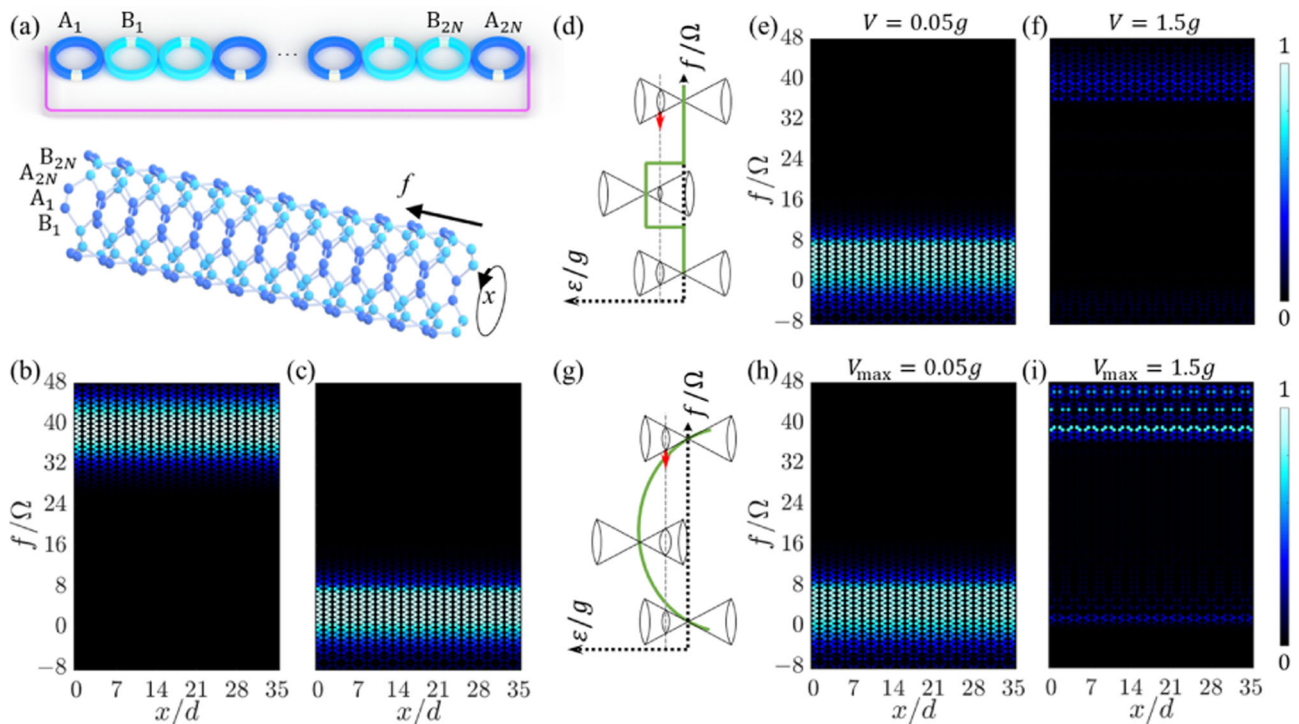
Fig. 2 Klein tunneling. a An external waveguide connects the first (A_1) and last (A_{2N}) ring resonator together, which forms an effective carbon-nanotube-like honeycomb lattice in the synthetic space with spatial direction (*x*) being periodic and frequency dimension (*f*) being finite. *N* is the number of groups of rings. **b** The intensity distribution in the synthetic lattice of the initial plane-wave excitation at propagation time $t = 0$. Ω is the free spectral range, and *d* denotes the horizontal distance between two sites with the same types in the synthetic lattice. **c** The intensity distribution in the synthetic lattice at $t = 42g^{-1}$ with no barrier, with *g* being the effective hopping amplitude. **d** The cartoon of the excited wave packet in the Dirac cone moving towards the negative direction along square-shape potential barrier (green line) with the frequency detuning ε (dashed gray line). The corresponding intensity distribution in the synthetic lattice with the square-shape potential barrier in **d** at $t = 42g^{-1}$ with maximum potential value **e** $V = 0.05g$ and **f** $V = 1.5g$. **g** The cartoon of the excited wave packet in the Dirac cone moving towards the negative direction along parabola-shape potential barrier (green line) with the frequency detuning ε (dashed gray line). The corresponding intensity distribution in the synthetic lattice with the parabola-shape potential barrier in **g** at $t = 42g^{-1}$ with maximum potential value **h** $V_{max} = 0.05g$ and **i** $V_{max} = 1.5g$. The red arrows in **d** and **g** present the direction of velocity.
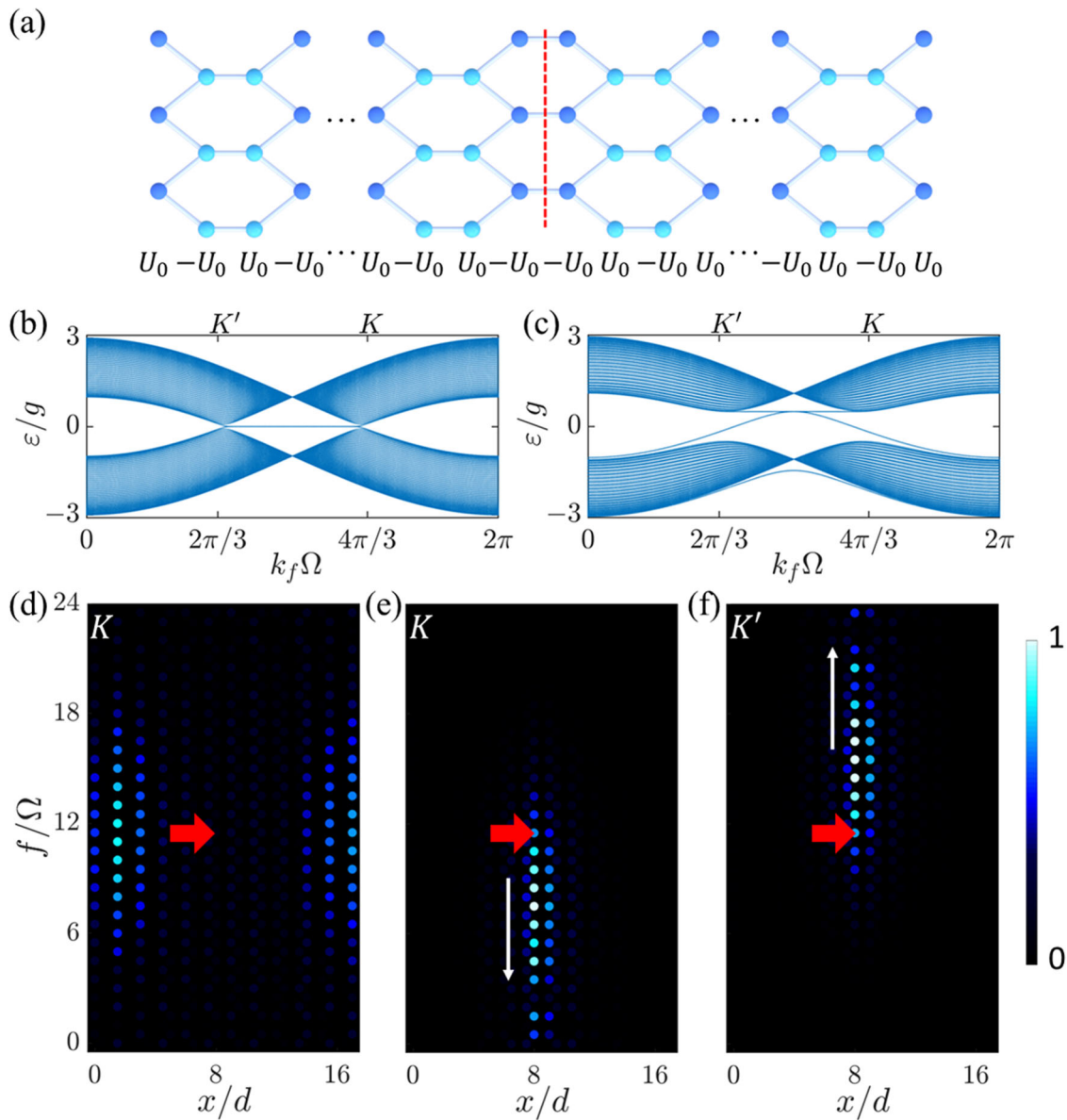
on-site potentials $\pm U_0$ alternatively in each ring except for the middle two rings having $-U_0$ forming the artificial domain wall. The band structures with an infinite frequency dimension and finite rings can be calculated. Figure 3b, c plots the projected band structures with potentials $U_0 = 0$ and $U_0 = 0.5g$, respectively. One sees that the Dirac point at K (K') with $k_f = 4\pi/3\Omega$ ($k_f = 2\pi/3\Omega$) is open and valley-dependent edge states are shown when effective on-site potentials are added.

To verify edge states in two valleys in the synthetic honeycomb lattice, we further assume that there are boundaries at the frequency dimension, which can be achieved either by adding auxiliary rings to knock out certain modes at particular frequency[56] or by designing a sharp change in the group velocity dispersion of the waveguide that composes the ring[30]. Therefore, a lattice with the range of $x \in [0, 17d]$ and $f \in [0, 23.5\Omega]$ is considered in simulations. We excite the 12th ring on the artificial domain wall by a source field which has the Gaussian spectrum: $s_2 = e^{ik_f \cdot (f - f_2)} \cdot e^{-(f - f_2)^2/\Delta^2}$, with $f_2 = 11.5\Omega$ and $\Delta = 8.49\Omega$. k_f here indicates the relative phase information for different frequency components in the source. We first choose $k_f = 4\pi/3\Omega$, which excites states near K point, and the simulation results at $t = 10g^{-1}$ with $U_0 = 0$ and $U_0 = 0.5g$ are plotted in Fig. 3d, e, respectively. One can see that when effective potentials are zero and the K point is degenerate, the field leaves the domain wall and spreads into the left and right sides of the synthetic lattice. On the other hand, when there are non-zero potentials shown in Fig. 3a, the one-way edge state at the K valley is excited and propagates towards lower frequency components with most of the energy

concentrated in the middle two rings on the artificial domain wall. Moreover, if we choose $k_f = 2\pi/3\Omega$ in the source to excite the edge state near the K' point, the field experience unidirectionally up-conversion in the middle two columns of the synthetic lattice [Fig. 3f], which shows the possibility of achieving valley-dependent edge states in the synthetic lattice.

Effective magnetic field. Photons are neutral particles, but it has been shown that, by introducing the proper distribution of hopping phases in a photonic lattice, one can create an effective magnetic field for photons[42]. In the synthetic honeycomb lattice in Fig. 1c, we consider the modulation phase as $\phi_{2n-1} = (2n - 1)\phi$ and $\phi_{2n} = (2n)\phi$. In each unit cell, the clockwise accumulation of the hopping phase is -2ϕ, which naturally brings an effective magnetic field. In Fig. 4a, we consider an infinite synthetic lattice and plot the projected band structure along ϕ, which gives the butterfly-like spectrum. The choice of phase can be tuned in each modulator arbitrarily. If we set $\phi = \pi/4$, a projected band structure along the k_f axis can be plotted by considering finite number of rings (with $n \in [1, 40]$). As shown in Fig. 4b, one can see that there are 8 bulk bands, which is consistent with the fact that there are 8 sites in each unit cell once phases with $\phi = \pi/4$ are considered. The middle two bulk bands have degenerate points. Meanwhile, there are 6 gaps between bulk bands, where it supports 8 pairs of topologically protected edge states. By analyzing the distribution of the eigenstate for each edge state, we can find whether the edge state is located on the left or right edge, as shown in Fig. 4b. Moreover, the Chern number for each bulk

Fig. 3 Valley-dependent edge state. a Effective on-site potentials (U_0 and $-U_0$) are alternatively applied in the synthetic lattice [formed by spatial dimension (x) and frequency dimension (f)], with an artificial domain wall in the middle two columns of synthetic lattices (labeled in red dashed line). The projected band structure in finite rings with **b** $U_0 = 0$, and **c** $U_0 = 0.5g$. k_f is the wave vector reciprocal to frequency axis, ε is the frequency shift of the field, Ω is the free spectral range, and g is the effective hopping amplitude. K and K' are two Dirac points. The simulated intensity distributions at propagation time $t = 10g^{-1}$ under conditions: **d** $U_0 = 0$, and $k_f = 4\pi/3\Omega$; **e** $U_0 = 0.5g$, and $k_f = 4\pi/3\Omega$; **f** $U_0 = 0.5g$, and $k_f = 2\pi/3\Omega$. d labels the horizontal distance between two sites with same types in the synthetic lattice. Red arrows indicate the excitation at the 12th ring with the central frequency mode at $f_2 = 11.5\Omega$. White arrows denote the unidirectional propagation.

band counting from the highest band can be calculated as 1, 1, -3, 2, -3, 1, 1, respectively.

We then perform simulations in a synthetic honeycomb lattice in 12 pairs of rings with $f \in [0, 11.5\Omega]$. To excite a specific edge state in Fig. 4b, we choose a single-frequency source field at the frequency $\omega_{m=5,A} + \omega_s$ near the 5th mode with a small detuning ω_s, i.e., $s_3 = e^{-i\omega_s t}$ and excite the rightmost ring. The simulations are performed with different parameters and results are plotted in Fig. 4c–f at $t = 20g^{-1}$. We first set $\phi = 0$, so there is no effective magnetic field, and choose $\omega_s = \varepsilon_1 = 0.9g$. One can see in Fig. 4c that the intensity distribution of the field undergoes a random-walk-like propagation in the synthetic honeycomb lattice, and bulk of the lattice is excited. Next, we set $\phi = \pi/4$ and introduce

the effective magnetic field. In this case, we again consider the excitation $\omega_s = \varepsilon_1$, and plot the result in Fig. 4d. Different from Fig. 4c, here one can see the topologically protected one-way edge state propagating towards lower frequency components at the right boundary, which is consistent with the negative slope of the edge state at ε_1 in Fig. 4b. We further use $\omega_s = \varepsilon_2 = 1.7g$ and $\omega_s = \varepsilon_3 = 2.2g$ to perform simulations and plot results in Fig. 4e, f, respectively. In both cases, the excited edge states propagate towards higher frequency components unidirectionally, corresponding to different edge states with the positive slope. Although we study phenomena only associated to the effective magnetic field with $\phi = \pi/4$, the gauge field can be easily tuned in this synthetic honeycomb lattice.
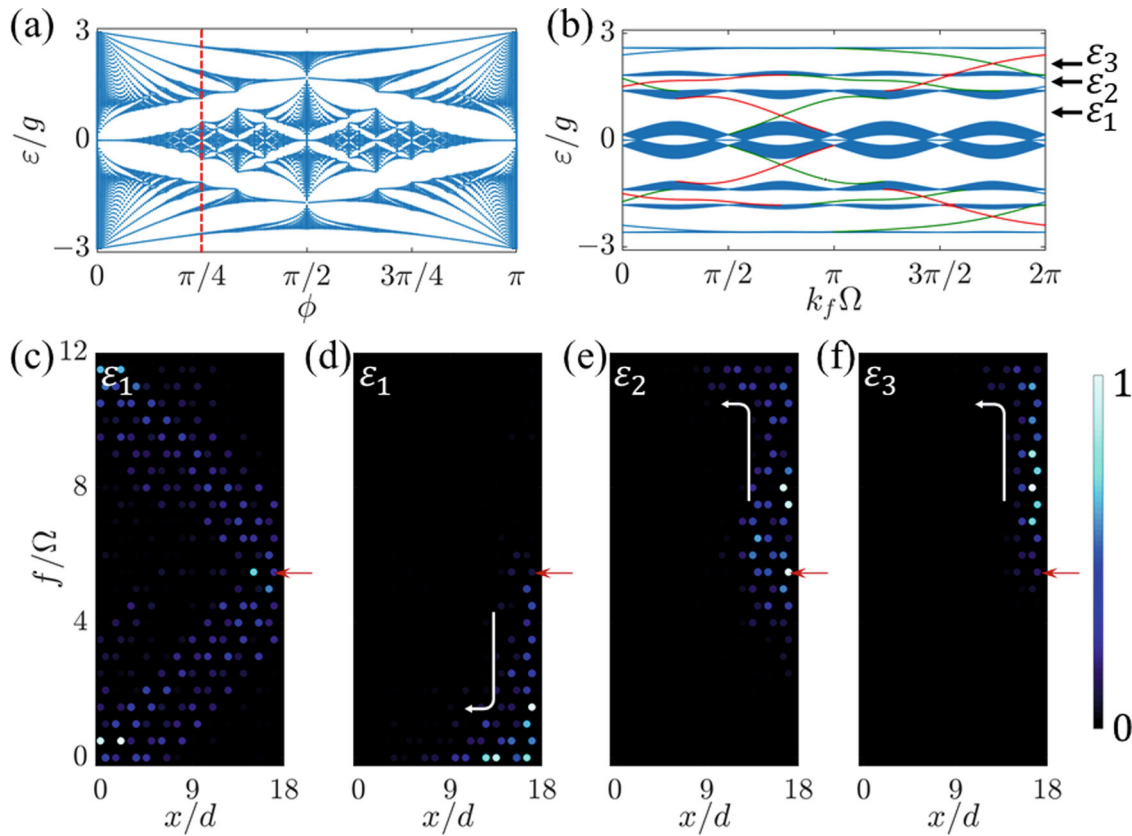
Fig. 4 Topological edge states with an effective magnetic field. a The projected band structure of the honeycomb lattice in Fig. 1c along modulation phase ϕ. The red dashed line refers to $\phi = \pi/4$. ε is the frequency shift of the field, and g is the effective hopping amplitude. **b** The projected band structure in finite rings with $\phi = \pi/4$, where k_f is the wave vector reciprocal to the frequency axis, and Ω is the free spectral range. Bands labeled in red (green) represents edge states on the right (left) boundary of the synthetic lattice. ε_1, ε_2, and ε_3 label three different frequencies in the band structure. **c** The simulated intensity distribution as a function of spatial dimension (x) and frequency dimension (f) at propagation time $t = 20g^{-1}$ with the input field having frequency shift $\omega_s = \varepsilon_1$ for the case $\phi = 0$. Simulated intensity distributions at $t = 20g^{-1}$ for the case $\phi = \pi/4$ with the input field having frequency shift ω_s being **d** ε_1, **e** ε_2, and **f** ε_3, respectively. d is the horizontal distance between two sites with the same types in the synthetic lattice. The red arrow indicates the $m = 5$th resonant frequency mode in the rightmost ring is excited. White arrows denote the unidirectional propagation.
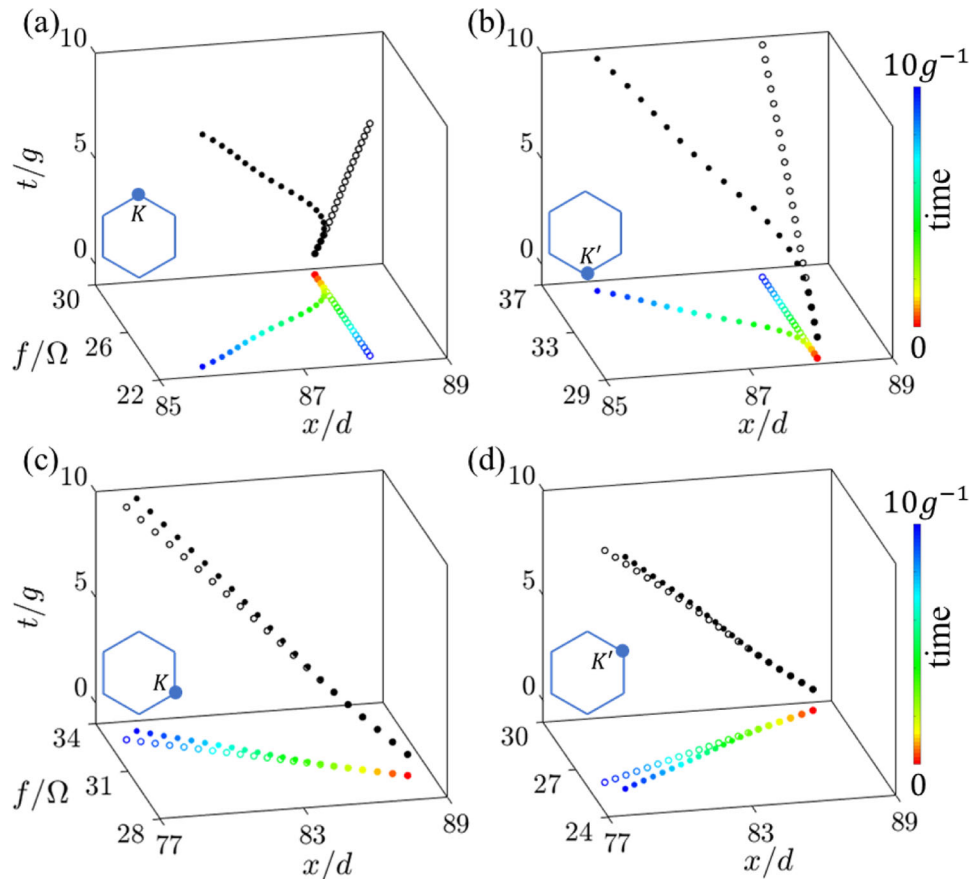
Valley-dependent Lorentz force. Different from the effective magnetic field for photons introduced by modulation phases, a pseudo magnetic field can also be alternatively generated by applying non-uniform strain in the honeycomb lattice[57]. In our proposed synthetic honeycomb lattice, we can also easily simulate the effective valley-dependent Lorentz force by varying modulation strength in each ring.

We consider a relatively large synthetic lattice composed of 56 pairs of rings with a range of $x \in [0, 83d]$ and $f \in [0, 59.5\Omega]$. We emphasize that, although there are 112 rings considered in simulations for better illustration, one does not require such a large number of rings to realize the effective valley-dependent Lorentz force in physics. For each modulator, we consider effective modulation strengths having $g_{2n-1} = [1 + \eta(3n - 42.75)]g$ and $g_{2n} = [1 + \eta(3n - 41.25)]g$, where η is a constant. Following the relation between coupling strengths in a honeycomb lattice and the effective gauge potential[58–60], we obtain an effective gauge potential $A_f(x) \propto g(x) - \kappa$ and $A_x = 0$ in the vicinity of the Dirac point, where the relation between n and x is used and κ is assumed to be a constant. This effective gauge potential leads to a pseudo magnetic field $B \propto \eta$ and along the z direction. Therefore, one can tune η by changing modulations strengths in rings to vary B in the synthetic honeycomb lattice.

In simulations, we inject fields into multiple rings with different frequency components to excite a Gaussian-shape wave packet

$s_4 = e^{-[(x-x_0)^2/(15.5d)^2+(f-f_3)^2/\Delta^2]} \cdot e^{i[k_x \cdot (x-x_0)+k_f(f-f_3)]}$ in the synthetic lattice, where $\Delta = 8.95\Omega$, $x_0 = 40d$ and $f_3 = 29.5\Omega$ are the center position of the Gaussian-shape wave packet. The phase information (k_x, k_f) is chosen to excite different states in the vicinity of the Dirac point K or K' in the first Brillouin zone. The simulated motion of the center of the wave packet (x_c, f_c) is then plotted to show the trajectory of the field in the synthetic lattice, with the definition of (x_c, f_c) can be found in Methods.

We first excite the vicinity of Dirac point by a wave packet s_4 with $(k_x, k_f) = (0, 4.4\pi/3\Omega)$ which gives an initial group velocity pointing toward the negative frequency axis. Without the pseudo magnetic field ($\eta = 0$), the wave packet of the field propagates without changing the direction and its trajectory is straight, as shown in Fig. 5a. Instead, if $\eta = 0.004$, the motion of the wave packet is bent to the clockwise side due to the pseudo magnetic field. On the other hand, if we excite the K' point with $(k_x, k_f) = (0, -4.4\pi/3\Omega)$, the motion of the wave packet is bent to the counter clockwise side under pseudo magnetic field in the synthetic lattice [Fig. 5b]. In Fig. 5c, d, we also excite the vicinity of Dirac points K and K' with $(k_x, k_f) = (2.2\sqrt{3}\pi/3\Omega, -2.2\pi/3\Omega)$ and $(2.2\sqrt{3}\pi/3\Omega, 2.2\pi/3\Omega)$, respectively. One see that, with a non-zero η, trajectories of the field are bent towards different directions. The direction of the pseudo magnetic field is dependent on the valley in the synthetic honeycomb lattice, which therefore results in the field bending effect by the effective valley-dependent Lorentz force.

Fig. 5 Valley-dependent Lorentz force. The simulated trajectories of the center of the Gaussian-shape wave packet (x_c, f_c) at discrete times with time interval $\delta t = 0.5g^{-1}$, where g is the effective hopping amplitude. The lattice is excited by initial source in the vicinity of the Dirac point K or K' with **a** $(k_x, k_f) = (0, 4.4\pi/3\Omega)$, **b** $(k_x, k_f) = (0, -4.4\pi/3\Omega)$, **c** $(k_x, k_f) = (2.2\sqrt{3}\pi/3\Omega, -2.2\pi/3\Omega)$, and **d** $(k_x, k_f) = (2.2\sqrt{3}\pi/3\Omega, 2.2\pi/3\Omega)$. k_x and k_f are wave vectors reciprocal to spatial and frequency axes, Ω is the free spectral range, d denotes the horizontal distance between two sites with the same types in the synthetic lattice, and t is propagation time. The trajectory with a black solid (hollow) circle represents the motion of the wave packet in the case with (without) the valley-dependent Lorentz force, which is projected into the spatial-frequency (x, f) plane with the varying color of circles representing the center position in the synthetic lattice at different simulation times.

Discussion

The highly tunable parameters of modulated ring resonators are of apparent significance in our theoretical design for achieving the synthetic honeycomb lattice, which can be realized in potential experiments based on established platforms with fiber loops[41–44], and lithium niobate technologies[45,61]. For the fiber-based ring resonator, the modulation frequency is ~10 MHz for a fiber length of ~10 m. 2 × 2 fiber couplers with a high-contract splitting ratio can be used to couple two rings. As for the on-chip lithium niobate device, fields in nearby resonators are coupled through the evanescent wave, where the modulation frequency can reach ~10 GHz when the ring radius is ~2–3 mm[45]. In our theoretical proposal, the hopping amplitude g_i as well as modulation phase ϕ_i along the frequency dimension [Fig. 1c] can be individually tuned by changing the external applied voltage on the electro-optic modulator inside each ring. Moreover, lengths of rings can be slightly altered by additional delay lines or thermal effects added into fiber or on-chip rings if needed, which provides a way to modify the effective on-site potential in each ring. Therefore, after the one-dimensional coupled rings are fabricated, this design can support simulating various graphene dynamics in two dimensions by setting proper parameters in modulators, including phenomena we have shown previously in this paper. Our proposed synthetic honeycomb lattice hence potentially provides high reconfigurability.

Here we study the proposal for constructing the honeycomb lattice in the synthetic space. In spatial dimensions, there naturally exist various lattice structures with different symmetries, which are possible to be simulated in the synthetic space. For example, different lattice-geometry opportunities have been theoretically discussed in the cold-atom platform where Raman-assisted tunnelings have been used to construct the synthetic dimension[62]. In photonics, however, most researches on synthetic dimensions focus on lattices with the C_4 symmetry[33,47,63], while constructing more complicated lattice structures is still lacking. The proposed method that we use to build the synthetic honeycomb lattice through staggered resonances, therefore, offers a different perspective for considering to create lattices with C_3 symmetry[64–67], such as triangular lattice and kagome lattice, where valley degree of freedom naturally emerges, and hence shows a way for further constructing other complicated lattice structures with richer physics in photonics[68,69].

In summary, we use an array of ring resonators composed by two types of rings undergoing dynamic modulations to form a two-dimensional honeycomb lattice in a synthetic space including one spatial dimension and one frequency dimension. We theoretically demonstrate a highly re-configurable synthetic honeycomb lattice, which is flexibly adjusted for achieving various parameters by changing the external modulation details. It has been used to simulate various phenomena including Klein

tunneling, valley-dependent edge states, topological edge states with an effective magnetic field, and field bending with the valley-dependent Lorentz force. Follow our theoretical proposal, future works can land on extending the honeycomb lattice to a three-dimensional structure with synthetic dimensions and/or adding optical nonlinearity to explore further light-manipulating opportunities. Our work shows not only the capability for simulating quantum phenomena, valley-dependent physics, and topological states in a modulated ring system, but also points out an alternative way to control the frequency information of light with synthetic dimensions, which potentially enriches quantum simulations of graphene physics with photonic technologies.

Methods

The construction of the synthetic honeycomb lattice. In Fig. 1a, ring A (B) supports a set of resonant modes with frequency $\omega_{m,A} = \omega_0 + m\Omega$ ($\omega_{m,B} = \omega_0 - \Omega/2 + m\Omega$), which is plotted in blue (cyan) color. The effective hopping amplitude between the nearby resonant modes a and b in two rings is formed through a two-step process: the resonant mode a in ring A couples to a corresponding non-resonant mode in ring B via evanescent-wave coupling, and then couples to the resonant mode b in ring B via the dynamic modulation, vice versa. Hence the effective coupling strength g is composed of both the evanescent-wave coupling strength and the modulation strength in EOM[70], and hence such connections construct a synthetic frequency dimension in a pairs of modulated rings. The construction of effective couplings between resonant modes in a pair of rings with the AB type can also be generalized to the pair of rings with the BA type by mirror symmetry [see the pair of rings labeled by $n = 1$ and $\alpha = 2$ as an example in Fig. 1c]. Therefore, in an array of pairs of rings arranged with alternate combinations AB and BA as shown in Fig. 1b, the spatially nearby resonant modes at the same frequency can be coupled through the evanescent wave with the coupling strength κ. Following this procedure, a synthetic honeycomb lattice can be constructed in a space shown in Fig. 1c with the longitudinal frequency dimension and the horizontal spatial dimension.

Simulation method. We expand the field inside each ring as

$$|\psi(t)\rangle = \sum_{n,m} \left(C_{n,m,\alpha} a^\dagger_{n,m,\alpha} + D_{n,m,\alpha} b^\dagger_{n,m,\alpha} \right)|0\rangle, \tag{2}$$

where $C_{n,m,\alpha}$ and $D_{n,m,\alpha}$ are the field amplitude at the mth mode in the corresponding ring. Schrödinger equation $i|\dot{\psi}(t)\rangle = H|\psi(t)\rangle$ is then used in simulations[30]. For different simulations, we take different source s to excite particular rings at specific modes, which we show details in the main text. The excitation process is done by coupling each ring with external waveguides where the light can be injected. The field amplitudes in rings can then also be read out through waveguides. The coupling equation between the external waveguide and the ring is

$$\begin{pmatrix} C_{n,m,\alpha}(D_{n,m,\alpha})(t^+) \\ E_{C(D),m,\alpha}(t^+) \end{pmatrix} = \begin{pmatrix} \sqrt{1-\gamma^2} & -i\gamma \\ -i\gamma & \sqrt{1-\gamma^2} \end{pmatrix} \begin{pmatrix} C_{n,m,\alpha}(D_{n,m,\alpha})(t^-) \\ E_{C(D),m,\alpha}(t^-) \end{pmatrix}, \tag{3}$$

where γ is the coupling strength between the external waveguide and the ring through evanescent wave. $E_{C(D),m,\alpha}(t^-)$ ($E_{C(D),m,\alpha}(t^+)$) is the corresponding field component injected (collected) through the external waveguide, and $t^\pm = t + 0^\pm$.

An effective on-site potential induced by frequency shift. For a ring, the resonant frequency for the mth resonant mode is $\omega_m = \omega_0 + m\Omega = \omega_0 + m \cdot 2\pi v_g/L$, where ω_0 is a reference optical frequency and is much larger than Ω (which is usually in the regime of GHz to THz). Without loss of generality, we can rewrite the equation of resonant frequency as $\omega_m = (M + m) \cdot 2\pi v_g/L$, where $M \gg m$ is a number orders of magnitudes larger than m. If we consider the length of the ring changes to $L' = L - \delta L$ ($\delta L \ll L$), the new resonant frequency becomes $\omega'_m = (M + M \cdot \delta L/L + m) \cdot 2\pi v_g/L = (M' + m') \cdot 2\pi v_g/L = \omega'_0 + m'\Omega$ under the first-order approximation, where $m' = m + \text{round}(M \cdot \delta L/L)$ and then M' is shifted by a number smaller than 1. Hence, by changing the length of rings slightly, one is possible to shift the reference frequency ω_0 with a small amount, which results in an effective on-site potential $U \equiv \omega'_0 - \omega_0$ in each ring.

Definitions of x_c and f_c. We define central positions of the Gaussian-shape wave packet in the synthetic lattice as

$$x_c = \frac{\sum_{n,m,\alpha} x_{n,m,\alpha} I_{m,n,\alpha}}{\sum_{n,m,\alpha} I_{n,m,\alpha}},$$
$$f_c = \frac{\sum_{n,m,\alpha} f_{n,m,\alpha} I_{m,n,\alpha}}{\sum_{n,m,\alpha} I_{n,m,\alpha}}, \tag{4}$$

where $I_{n,m,\alpha} = |C_{n,m,\alpha}|^2$ or $|D_{n,m,\alpha}|^2$, $x_{n,m,\alpha}$, and $f_{n,m,\alpha}$ are the corresponding position along the x axis and frequency dimension in the synthetic lattice, respectively.

References

1. Castro Neto, A. H., Guinea, F., Peres, N. M. R., Novoselov, K. S. & Geim, A. K. The electronic properties of graphene. *Rev. Mod. Phys.* **81**, 109–162 (2009).
2. Das Sarma, S., Adam, S., Hwang, E. H. & Rossi, E. Electronic transport in two-dimensional graphene. *Rev. Mod. Phys.* **83**, 407–470 (2011).
3. Zhang, H. J. et al. Topological insulators in ternary compounds with a honeycomb lattice. *Phys. Rev. Lett.* **106**, 156402 (2011).
4. Kitagawa, K. et al. A spin–orbital-entangled quantum liquid on a honeycomb lattice. *Nature* **554**, 341–345 (2018).
5. Tarruell, L., Greif, D., Uehlinger, T., Jotzu, G. & Esslinger, T. Creating, moving and merging Dirac points with a Fermi gas in a tunable honeycomb lattice. *Nature* **483**, 302–305 (2012).
6. Milićević, M. et al. Edge states in polariton honeycomb lattices. *2D Mater.* **2**, 034012 (2015).
7. Bahat-Treidel, O. et al. Klein tunneling in deformed honeycomb lattices. *Phys. Rev. Lett.* **104**, 063901 (2010).
8. Rechtsman, M. C. et al. Strain-induced pseudomagnetic field and photonic Landau levels in dielectric structures. *Nat. Photonics* **7**, 153–158 (2013).
9. Ezawa, M. Spin valleytronics in silicene: quantum spin Hall-quantum anomalous Hall insulators and single-valley semimetals. *Phys. Rev. B* **87**, 155415 (2013).
10. Ozawa, T. & Carusotto, I. Anomalous and quantum Hall effects in lossy photonic lattices. *Phys. Rev. Lett.* **112**, 133902 (2014).
11. Jacqmin, T. et al. Direct observation of Dirac cones and a Flatband in a honeycomb lattice for polaritons. *Phys. Rev. Lett.* **112**, 116402 (2014).
12. Deng, F. et al. Valley-dependent beams controlled by pseudomagnetic field in distorted photonic graphene. *Opt. Lett.* **40**, 3380–3383 (2015).
13. Dong, J. W., Chen, X. D., Zhu, H., Wang, Y. & Zhang, X. Valley photonic crystals for control of spin and topology. *Nat. Mater.* **16**, 298–302 (2017).
14. Jiang, X. et al. Direct observation of Klein tunneling in phononic crystals. *Science* **370**, 1447–1450 (2020).
15. Jamadi, O. et al. Direct observation of photonic Landau levels and helical edge states in strained honeycomb lattices. *Light Sci. Appl.* **9**, 144 (2020).
16. Noh, J., Huang, S., Chen, K. P. & Rechtsman, M. C. Observation of photonic topological valley hall edge states. *Phys. Rev. Lett.* **120**, 063902 (2018).
17. Guan, C. et al. Pseudospin-mediated optical spin–spin interaction in nonlinear photonic graphene. *Laser Photonics Rev.* **13**, 1800242 (2019).
18. Barik, S. et al. A topological quantum optics interface. *Science* **359**, 666–668 (2018).
19. Lin, H. & Lu, L. Dirac-vortex topological photonic crystal fiber. *Light Sci. Appl.* **9**, 202 (2020).
20. Yang, Z. Q., Shao, Z. K., Chen, H., Mao, X. R. & Ma, R. M. Spin-momentum-locked edge mode for topological vortex lasing. *Phys. Rev. Lett.* **125**, 013903 (2020).
21. Zhang, Z. et al. Observation of edge solitons in photonic graphene. *Nat. Commun.* **11**, 1902 (2020).
22. Rechtsman, M. C. et al. Photonic Floquet topological insulators. *Nature* **496**, 196–200 (2013).
23. Parappurath, N., Alpeggiani, F., Kuipers, L. & Verhagen, E. Direct observation of topological edge states in silicon photonic crystals: Spin, dispersion, and chiral routing. *Sci. Adv.* **6**, eaaw4137 (2020).
24. Klembt, S. et al. Exciton-polariton topological insulator. *Nature* **562**, 552–556 (2018).
25. Smirnova, D. et al. Third-Harmonic generation in photonic topological metasurfaces. *Phys. Rev. Lett.* **123**, 103901 (2019).
26. Yuan, L., Lin, Q., Xiao, M. & Fan, S. Synthetic dimension in photonics. *Optica* **5**, 1396–1405 (2018).
27. Ozawa, T. & Price, H. M. Topological quantum matter in synthetic dimensions. *Nat. Rev. Phys.* **1**, 349–357 (2019).

28. Lustig, E. & Segev, M. Topological photonics in synthetic dimensions. *Adv. Opt. Photon.* **13**, 426–461 (2021).
29. Yuan, L., Dutt, A. & Fan, S. Tutorial: synthetic frequency dimensions in dynamically modulated ring resonators. *APL Photonics* **6**, 071102 (2021).
30. Yuan, L., Shi, Y. & Fan, S. Photonic gauge potential in a system with a synthetic frequency dimension. *Opt. Lett.* **41**, 741–744 (2016).
31. Ozawa, T., Price, H. M., Goldman, N., Zilberberg, O. & Carusotto, I. Synthetic dimensions in integrated photonics: from optical isolation to four-dimensional quantum Hall physics. *Phys. Rev. A* **93**, 043827 (2016).
32. Lin, Q., Sun, X. Q., Xiao, M., Zhang, S. C. & Fan, S. A three-dimensional photonic topological insulator using a two-dimensional ring resonator lattice with a synthetic frequency dimension. *Sci. Adv.* **4**, eaat2774 (2018).
33. Lustig, E. et al. Photonic topological insulator in synthetic dimensions. *Nature* **567**, 365–360 (2019).
34. Yu, D., Yuan, L. & Chen, X. Isolated photonic flatband with the effective magnetic flux in a synthetic space including the frequency dimension. *Laser Photonics Rev.* **14**, 2000041 (2020).
35. Yang, Z. et al. Mode-locked topological insulator laser utilizing synthetic dimensions. *Phys. Rev. X* **10**, 011059 (2020).
36. Song, Y. et al. Two-dimensional non-Hermitian skin effect in a synthetic photonic lattice. *Phys. Rev. Appl.* **14**, 064076 (2020).
37. Dutt, A., Minkov, M., Williamson, I. A. D. & Fan, S. Higher-order topological insulators in synthetic dimensions. *Light Sci. Appl.* **9**, 131 (2020).
38. Zhang, W. & Zhang, X. Quadrupole topological phases in the zero-dimensional optical cavity. *EPL* **131**, 24004 (2020).
39. Nemirovsky, L., Cohen, M., Lumer, Y., Lustig, E. & Segev, M. Synthetic-space photonic topological insulators utilizing dynamically invariant structure. *Phys. Rev. Lett.* **127**, 093901 (2021).
40. Poo, Y., Wu, R. X., Lin, Z., Yang, Y. & Chan, C. T. Experimental realization of self-guiding unidirectional electromagnetic edge states. *Phys. Rev. Lett.* **106**, 093903 (2011).
41. Dutt, A. et al. Experimental band structure spectroscopy along a synthetic dimension. *Nat. Commun.* **10**, 3122 (2019).
42. Dutt, A. et al. A single photonic cavity with two independent physical synthetic dimensions. *Science* **367**, 59–64 (2020).
43. Li, G. et al. Dynamic band structure measurement in the synthetic space. *Sci. Adv.* **7**, eabe4335 (2021).
44. Wang, K. et al. Generating arbitrary topological windings of a non-Hermitian band. *Science* **371**, 1240–1245 (2021).
45. Hu, Y., Reimer, C., Shams-Ansari, A., Zhang, M. & Loncar, M. Realization of high-dimensional frequency crystals in electro-optic microcombs. *Optica* **7**, 1189 (2020).
46. Ozawa, T. et al. Topological photonics. *Rev. Mod. Phys.* **91**, 015006 (2019).
47. Segev, M. & Bandres, M. A. Topological photonics: where do we go from here? *Nanophotonics* **10**, 425–434 (2021).
48. Pérez, D. et al. Multipurpose silicon photonics signal processor core. *Nat. Commun.* **8**, 636 (2017).
49. Nakajima, M., Tanaka, K. & Hashimoto, T. Scalable reservoir computing on coherent linear photonic processor. *Commun. Phys.* **4**, 20 (2021).
50. Feng, L. T. et al. On-chip coherent conversion of photonic quantum entanglement between different degrees of freedom. *Nat. Commun.* **7**, 11985 (2016).
51. Liu, C. et al. Two-dimensional materials for next-generation computing technologies. *Nat. Nanotechnol.* **15**, 545–557 (2020).
52. Dreisow, F. et al. Klein tunneling of light in waveguide superlattices. *EPL* **91**, 10008 (2012).
53. Ni, X. et al. Spin-and valley-polarized one-way Klein tunneling in photonic topological insulators. *Sci. Adv.* **4**, eaap8802 (2018).
54. Shan, Q., Yu, D., Li, G., Yuan, L. & Chen, X. One-way topological states along vague boundaries in synthetic frequency dimensions including group velocity dispersion. *PIER* **169**, 33–43 (2020).
55. Turner, A. C. et al. Tailored anomalous group-velocity dispersion in silicon channel waveguides. *Opt. Express* **14**, 4357–4365 (2006).
56. Yuan, L. et al. Photonic gauge potential in one cavity with synthetic frequency and orbital angular momentum dimensions. *Phys. Rev. Lett.* **122**, 083903 (2019).
57. Low, T. & Guinea, F. Strain-induced pseudomagnetic field for novel graphene electronics. *Nano Lett.* **10**, 3551–3554 (2010).
58. Vozmediano, M. A. H., Katsnelson, M. I. & Guinea, F. Gauge fields in graphene. *Phys. Rep.* **496**, 109–148 (2010).
59. de Juan, F., Cortijo, A., Vozmediano, M. A. H. & Cano, A. Aharonov-Bohm interferences from local deformations in graphene. *Nat. Phys.* **7**, 810–815 (2011).
60. Prabhakar, S., Nepal, R., Melnik, R. & Kovalev, A. A. Valley-dependent Lorentz force and Aharonov-Bohm phase in strained graphene p-n junction. *Phys. Rev. B* **99**, 094111 (2019).
61. Zhang, M., Wang, C., Cheng, R., Shams-Ansari, A. & Lončar, M. Monolithic ultra-high-Q lithium niobate microring resonator. *Optica* **4**, 1536–1537 (2017).
62. Suszalski, D. & Zakrzewski, J. Different lattice geometries with a synthetic dimension. *Phys. Rev. A* **94**, 033602 (2016).
63. Ozawa, T. & Price, H. M. Topological quantum matter in synthetic dimensions. *Nat. Rev. Phys.* **1**, 349–357 (2019).
64. Zandbergen, S. R. & de Dood, M. J. A. Experimental observation of strong edge effects on the pseudodiffusive transport of light in photonic graphene. *Phy. Rev. Lett.* **104**, 043903 (2010).
65. Struck, J. et al. Quantum simulation of frustrated classical magnetism in triangular optical lattices. *Science* **333**, 996–999 (2011).
66. Schulz, S. A., Upham, J., O'Faolain, L. & Boyd, R. W. Photonic crystal slow light waveguides in a kagome lattice. *Opt. Lett.* **42**, 3243–3246 (2017).
67. Li, M. et al. Higher-order topological states in photonic kagome crystals with long-range interactions. *Nat. Photonics* **14**, 89–94 (2019).
68. Chern, G. & Saxena, A. PT-symmetric phase in kagome-based photonic lattices. *Opt. Lett.* **40**, 5806–5809 (2015).
69. Maimaiti, W., Dietz, B. & Andreanov, A. Microwave photonic crystals as an experimental realization of a combined honeycomb-kagome lattice. *Phys. Rev. B* **102**, 214301 (2020).
70. Yuan, L., Xiao, M., Lin, Q. & Fan, S. Synthetic space with arbitrary dimensions in a few rings undergoing dynamic modulation. *Phys. Rev. B* **97**, 104105 (2018).

Acknowledgements

Author contributions

L.Y. initiated the idea. D.Y. and L.Y. performed simulations. D.Y., G.L., M.X., and L.Y. discussed the results. D.Y., G.L., and L.Y. wrote the draft. D.Y., G.L., M.X., D.-W.W., Y.W., L.Y., and X.C. revised the manuscript and contributed to scientific discussions of the manuscript. L.Y. and X.C. supervised the project.

Competing interests

The authors declare no competing interests.

Additional information

Correspondence and requests for materials should be addressed to Luqi Yuan.

Peer review information *Communications Physics* thanks the anonymous reviewers for their contribution to the peer review of this work.

Reprints and permission information is available at http://www.nature.com/reprints

Publisher's note Springer Nature remains neutral with regard to jurisdictional claims in published maps and institutional affiliations.